Aluminum Exchange between Citrate and Human Serum Transferrin and Interaction with Transferrin Receptor 1

ARTICLE *in* BIOCHEMISTRY · APRIL 2003

Impact Factor: 3.02 · DOI: 10.1021/bi020627p · Source: PubMed

4 AUTHORS, INCLUDING:

Miryana Hémadi
French National Centre for Scientific Research
25 PUBLICATIONS **378** CITATIONS
SEE PROFILE

Philippe Kahn
French National Centre for Scientific Research
27 PUBLICATIONS **336** CITATIONS
SEE PROFILE

Aluminum Exchange between Citrate and Human Serum Transferrin and Interaction with Transferrin Receptor 1

Miryana Hémadi, Geneviève Miquel, Philippe H. Kahn, and Jean-Michel El Hage Chahine*

Interfaces, Traitements, Organisation et Dynamique des Systèmes, Université Paris 7-CNRS UMR 7086, 1, rue Guy de la Brosse, 75005 Paris, France

Received October 11, 2002; Revised Manuscript Received December 12, 2002

ABSTRACT: The kinetics and thermodynamics of Al(III) exchange between aluminum citrate (AlL) and human serum transferrin were investigated in the 7.2−8.9 pH range. The C-site of human serum apotransferrin in interaction with bicarbonate removes Al(III) from Al citrate with an exchange equilibrium constant $K_1 = (2.0 \pm 0.6) \times 10^{-2}$; a direct second-order rate constant $k_1 = 45 \pm 3\ M^{-1}\ s^{-1}$; and a reverse second-order rate constant $k_{-1} = (2.3 \pm 0.5) \times 10^3\ M^{-1}\ s^{-1}$. The newly formed aluminum−protein complex loses a single proton with proton dissociation constant $K_{1a} = (15 \pm 3)$ nM to yield a first kinetic intermediate. This intermediate then undergoes a modification in its conformation followed by two proton losses; first-order rate constant $k_2 = (4.20 \pm 0.02) \times 10^{-2}\ s^{-1}$ to produce a second kinetic intermediate, which in turn undergoes a last slow modification in the conformation to yield the aluminum-loaded transferrin in its final state. This last process rate-controls Al(III) uptake by the N-site of the protein and is independent of the experimental parameters with a constant reciprocal relaxation time $\tau_3^{-1} = (6 \pm 1) \times 10^{-5}\ s^{-1}$. The affinities involved in aluminum uptake by serum transferrins are about 10 orders of magnitude lower than those involved in the uptake of iron. The interactions of iron-loaded transferrins with transferrin receptor 1 occur with average dissociation constants of 3 ± 1 and 5 ± 1 nM for the only C-site iron-loaded and of 6.0 ± 0.6 and 7 ± 0.5 nM for the iron-saturated ST in the absence or presence of CHAPS, respectively. No interaction is detected between receptor 1 and aluminum-saturated or mixed C-site iron-loaded/N-site aluminum-loaded transferrin under the same conditions. The fact that aluminum can be solubilized by serum transferrin in biological fluids does not necessarily imply that its transfer from the blood stream to cytoplasm follows the receptor-mediated pathway of iron transport by transferrins.

Transferrins are considered as the most essential iron transport system in vertebrates and invertebrates. They are also present in some bacteria (*1*). These proteins belong to the superfamily of transferrins that includes periplasmic transport proteins (*2*). Most of the transferrins as well as human transferrin (ST)[1] consist of a single polypeptide chain of about 700 amino acids organized in two lobes (−C and −N) linked by an interlobe chain. Each lobe consists of two domains containing four protein ligands to which iron is coordinated. Iron is also coordinated to a synergistic carbonate anion without which the protein loses its affinity for the metal (*3*−*5*). When the protein is in the iron-free state, the two lobes are mostly in an open conformation (apoform), whereas they are in a closed conformation when the protein is iron-loaded (*4*). In mammals, ST solubilizes iron(III) in neutral biological media. When it becomes iron-loaded, it is recognized by the transferrin receptor 1 (TFR) and is internalized in the cytoplasm by receptor-mediated endocytosis (*6*). The adduct formed by iron-loaded ST in interaction with TFR is the major iron transport system in vertebrates and invertebrates. Transferrins can also bind other nonferric metallic elements such as aluminum (*7*−*11*). These proteins are, therefore, considered as possible vehicles for aluminum from bloodstream to cytosol (*12*, *13*).

Aluminum is the most abundant metallic element in the earth's crust. It was until the beginning of the last century rather inaccessible to living species, and therefore, considered innocuous. However, its release from soils by acid rain and its extensive use in food packaging and water processing increased its bio-availability to such an extent that exposure to aluminum became inevitable (*14*). Aluminum is involved in dialysis dementia, is a neurotoxicant, and causes nephritic disorders and pulmonary fibrosis, etc. (*14*−*19*). However, its role in neurodegenerative diseases such as Alzheimer's

* To whom correspondence should be addressed. Phone: 33144276807. Fax: 33144276814. E-mail: chahine@paris7.jussieu.fr.

[1] Abbreviations: ST, serum transferrin; TFR, serum transferrin receptor 1; c_1, analytical serum transferrin concentration; c_2, aluminum citrate concentration; AlL, neutral aluminum monocitrate; L^{3-}, citrate anion; $H_2T'_N$-T'_CH_2, apotransferrin, both sites of which are in an unknown state of protonation and charge; $H_2T'_N$-T_CH_3 and T_CH_3, apotransferrin, only the C-site of which is interacting with bicarbonate; H_3T_N-T_CH_3, transferrin, both sites of which are interacting with bicarbonate; T, transferrin in an unknown state; T_CH_3Al, T_CH_2Al, T_C-Al, $H_JT_NT_CH_2Al$, $TH_{J+2}TAl$, TH_JAl, $T'H_JAl$, the different C-site species of aluminum-loaded serum transferrin in unknown state of charge, conformation, and protonation; TFe_2, holotransferrin in an unknown state; TAl_2, $T'H_JAl$, $T'H_JAl_2$, the different species of aluminum-saturated serum transferrin in unknown state of charge, conformation, and protonation; T_CH_3Fe, T_CHFe, $T_NH_3T_CH_2Fe$, TH_5Fe, $TH_{(5-l)}Fe$, $T'H_{(5-l)}Fe$, $T'H_{(4-l)}Fe$, $T''H_{(4-l)}Fe$, the different C-site species of iron-loaded serum transferrin in unknown states of charge, conformation, and protonation; $T'H_{(4-l)}Fe_2$, $T''H_{(4-l)}Fe_2$, the different species of iron-saturated serum transferrin in unknown states of charge, conformation, and protonation; TFR−$(TFe_2)_2$, receptor 1 in interaction with two holotransferrins.

10.1021/bi020627p CCC: $25.00
Published on Web 02/19/2003

is extremely controversial and has never been directly established (*17*, *20*). Aluminum transport in humans supposedly follows the iron transport pathway and would occur via the aluminum-loaded ST in interaction with TFR (*12*, *13*). The structure of TFR is now well-known (*21*). It is a homodimeric 190 kDa glycosylated membrane protein composed of an endodomain anchored in the plasma membrane and an ectodomain directed toward the biological fluids. The ectodomain can interact with two iron-loaded transferrins (*22*).

Aluminum forms stable complexes with citrate and even more stable complexes with ST (*7*, *23*). Therefore, transferrins appear to be the predominant aluminum carriers in biological fluids and across the blood brain barrier (*17*). Nevertheless, the mechanism of aluminum uptake by ST is not known, and most of the literature deals with the thermodynamic aspect of the uptake (*7*, *9*, *11*). Recently, by using the methods and techniques of chemical relaxation (*24*−*26*), we established a multistep mechanism for the uptake of iron by the three major transferrins: ST, lactoferrin, and ovotransferrin. In this mechanism, the first stage is the interaction of the C-site of the apotransferrin with bicarbonate. This interaction is indispensable for a first fast iron exchange between a chelate and the open conformation of the C-site. This iron uptake precedes a series of proton losses and changes in the conformation of the protein that leads to a second iron uptake at the N-site, and finally the protein attains its thermodynamic closed conformation in about 1−3 h (*5*, *27*).

We propose in this article a mechanism for aluminum exchange between its two potential carriers, citrate and human ST. We furthermore analyze the interaction of iron-saturated, aluminum-saturated, only C-site iron-loaded, and the mixed C-site iron-loaded/N-site aluminum-loaded transferrins with TFR.

EXPERIMENTAL PROCEDURES

Better than 98% pure human serum apotransferrin (Sigma) was further purified by published procedures; its purity was checked spectrophotometrically and by urea and SDS polyacrylamide gel electrophoresis (*28*−*30*). KCl (Merck Suprapur), NaOH, HCl (Merck Titrisol), EDTA (Merck Titriplex), $FeCl_3$, trisodium citrate, acetic acid (96%) (Merck), sodium bicarbonate, glycerol, urea, SDS, boric acid, 3-[(3-cholamidopropyl]dimethylammonio]-1-propane-sulfonate (CHAPS) (Ultra grade), dithiothreitol (DTT), phenylmethylsulfonylfluoride (PMSF), Triton TX-100, ethanolamine, glycine (electrophoresis reagent), sodium azide, blue dextran (Sigma), ammonium sulfate, nitrilotriacetic acid [$N(AcH)_3$], bromophenol blue, Brilliant blue, Hepes (Aldrich), acrylamide, APS, TEMED (Boehringer Mannheim), dibasic potassium-phosphate, trihydrate (Calbiochem), NaCl (molecular biology grade from Merck), Sephadex G100 super fine and G50 (Pharmacia), and aluminum chloride (Riedel-de-Haen puriss.) were used without further purification. Desferrioxamine was a gift from Novartis. Water and glassware were prepared as described previously (*28*).

Stock Solutions. All stock solutions were prepared in previously boiled doubly distilled water, sterilized afterward at 120 °C, and used fresh. Phosphate buffer saline (PBS) was prepared from dibasic potassium phosphate trihydrate and NaCl. The Hepes concentration in neutral buffers ranged from 10 to 50 mM, and final pHs were adjusted to between 7 and 9 with micro quantities of concentrated HCl or NaOH. Transferrin concentrations (c_1) were spectrophotometrically checked and diluted further to the required final concentrations in the buffers (*28*). $FeNAc_3$ solutions were prepared as previously described (*28*). Neutral aluminum monocitrate AlL solutions (0.5 M) were prepared by first mixing one part of a neutral solution of trisodium citrate with one part of an equimolar solution of $AlCl_3$ at pH 2. The pH was slowly raised to 6 with micro quantities of 10 N NaOH. These solutions were further diluted to the required final aluminum monocitrate (AlL) concentrations in the final neutral buffers. The $NaHCO_3$ concentrations ranged from 5 to 30 mM in the apotransferrin and AlL solutions. All final ionic strengths in the Hepes buffers were adjusted to 0.2 M with KCl.

Metal-Loaded Transferrins. The iron-saturated serum transferrin and the transferrin in which only the C-site was iron-loaded were prepared as described elsewhere (*29*). Iron load was always checked by polyacrylamide−urea gel electrophoresis (*30*). Aluminum-saturated transferrin was obtained in the presence of 20 mM of bicarbonate by incubating apotransferrin at pH 7.4 for 48 h at 37 °C with more than 10 equiv of aluminum monocitrate. The presumably C-site aluminum-loaded ST was prepared by incubating ST for 48 h with 1 equiv of AlL in the neutral buffer and in the presence of 20 mM sodium bicarbonate. The mixed C-site iron-loaded and N-site aluminum ST was prepared by incubating for 48 h the C-site iron-loaded ST with 15 equiv of AlL in the neutral buffer and in the presence of 20 mM sodium bicarbonate. The protein solutions were dialyzed eight times against final buffers, and the aluminum load was checked by Inductive Plasma Coupling by Dr. J.-C. Rouchaud at the CECM laboratory of the CNRS in the city of Vitry.

TFR Purification. TFR was extracted from human placenta and purified on an Affigel 15 (Biorad) column doped with holotransferrin according to the published procedures and by following the Turkewicz et al. protocol as modified by Bali et al. (*31*, *32*). Purity was checked by gradient SDS−PAGE (*31*, *32*). TFR was obtained pure and used complete without cleaving the endodomain. Protein concentrations were determined spectrophotometrically and by a Bio-Rad protein assay. Final TFR varied from 4 to 6 mg per placenta. TFR solutions were dialyzed four times against the final buffer. Final TFR concentrations were achieved by dilution. Human placenta screened HIV-free and hepatitis-C free were provided by the maternity hospital of the city of Ivry.

Size-Exclusion Chromatography. Sephadex G100 Super Fine was boiled in a 10 mM Hepes, $\mu = 0.2$, and pH 7.80 buffer. The suspension was afterward kept at 4 °C after the addition of 0.1% sodium azide. The bed volume of the chromatography column was about 2 mL, the full elution volume was about 3.2 mL, the void volume was about 1 mL, and the elution fractions were 400 μL (40% of the void volume). The columns were washed with about 30 mL of buffer, and the proteins were only deposited when the absorption spectrum of the washing solution was identical to that of the buffer. All protein concentrations were 1 μM, the deposited volume was 100 μL, and the detection was spectrophotometric.

Spectrophotometric and Kinetic Measurements. Absorption measurements were performed at (25 ± 0.1) °C on a Cary 500 spectrophotometer equipped with a thermostated cell carrier. Fluorimetric measurements were performed at (25 ± 0.1) °C on a Aminco-Bowman series 2 luminescence spectrometer equipped with a thermostated cell carrier. Emission spectra were measured in the 300−420 nm range. Excitation wavelength was set to 280 nm (*27*). Fast kinetic measurements were performed on a SF 3L Hi-Tech stopped-flow spectrophotometer equipped with two different light sources and a thermostated bath at (25 ± 0.5) °C, as described previously (*5*, *27*).

Data Analysis. The data were investigated either by linear or nonlinear least-squares analysis. The uncertainties on the slopes and intercepts of the linear regressions are given as 3-fold the standard deviations (3σ). All the observed kinetics were pure mono- or multiexponential. They were analyzed as reported elsewhere and dealt with as relaxation modes (*28*).

RESULTS

All experimental conditions were set so as to allow the use of the methods and techniques of chemical relaxation (*26*). The state of protonation and charge of the protein species involved in aluminum uptake by ST in neutral media are unknown. Therefore, the charge of the protein species is not indicated, and the subscripts used for H are only relative values.

Kinetics of Metal Exchange between Aluminum−Monocitrate and ST. Complex formation between ST and Al(III) produces changes in the differential absorption and fluorescence emission spectra of the protein (*7*, *8*, *33*). These spectral changes are used to monitor the kinetics of metal exchange between the citrate chelate and the protein.

When a solution of apo-ST is rapidly mixed with a solution of Al(III) monocitrate, three kinetic processes are detected (Figure 1). They occur as exponential increases with time in the differential absorption (ΔA) at $\lambda = 240$ nm (ΔA is the difference between the absorption of the protein species in the presence of aluminum monocitrate and that of ST) or the fluorescence emission at an emission wavelength of $\lambda_{em} = 330$ nm with an excitation wavelength of $\lambda_{ex} = 280$ nm. The first process occurs in the 10−300 s range and leads to the accumulation of a first kinetic product (Figures 1a and 2). It is followed by the second process, which occurs in the 300−3000 s range and leads to the accumulation of a second kinetic intermediate (Figures 1b and 2). The third process occurs in the 6×10^4 s range (Figures 1c and 2). A stopped-flow investigation did not show any faster kinetic process than those reported in Figure 1.

Although with lower amplitudes, the two fast processes in Figure 1a,b occur equally with a ST of which only the C-site is iron-loaded and with a ST previously incubated for 48 h with 1 equiv of aluminum monocitrate (presumably aluminum-loaded at the C-site (*34*)). As for the third, slow process (Figure 1c), it is not observed during aluminum uptake by the C-site iron-loaded transferrin or the presumably C-site aluminum-loaded protein.

First Kinetic Process. At a constant ionic strength $\mu = 0.2$, the experimental reciprocal relaxation times (τ_1^{-1}) associated with the first kinetic process of Figure 1a depend

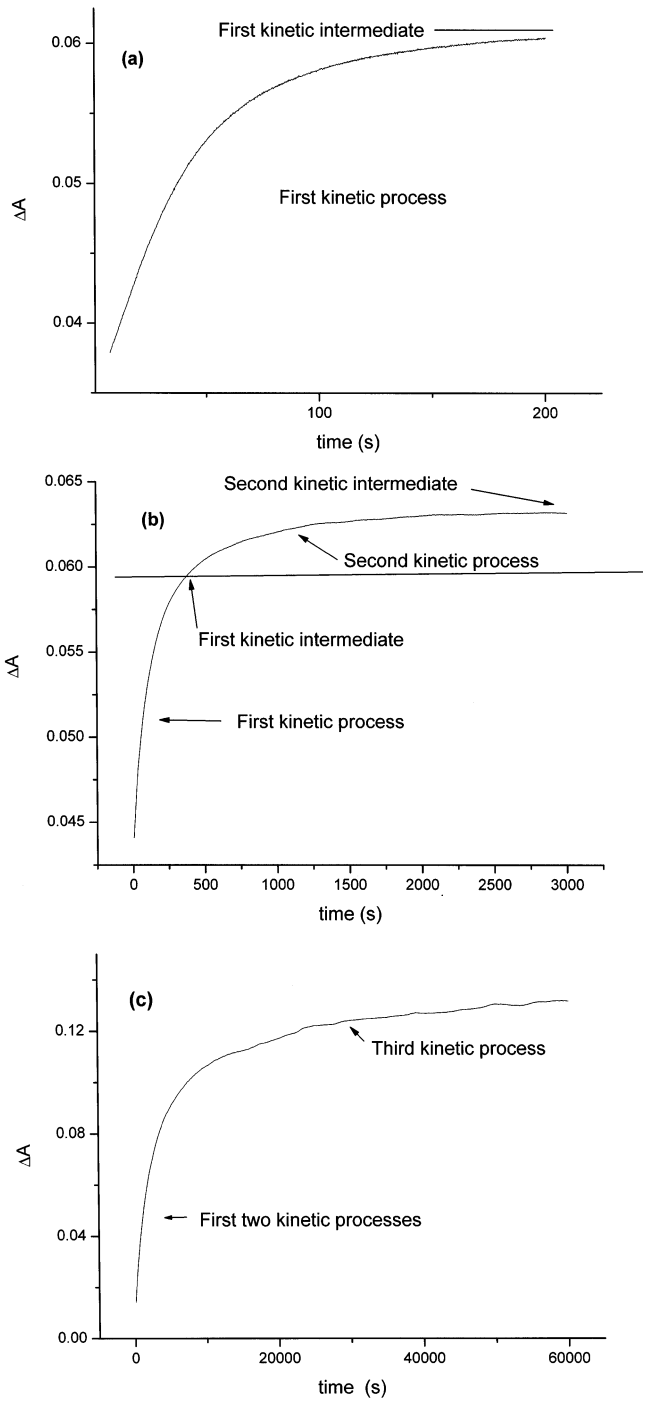

FIGURE 1: Variation of the differential absorption with time when a neutral solution of apo-ST (2 μM for a and b, and 5μM for c) is mixed with a neutral solution of aluminum citrate (0.5 mM) at pH 8.63 and 25 ± 0.5 °C with $[HCO_3^-] = 20$ mM and $\mu = 0.2$.

on the analytical concentrations of ST (c_1), aluminum monocitrate (c_2), $[HCO_3^-]$, and proton. Bicarbonate plays the role of a synergistic anion required for the uptake of aluminum (*11*). The interaction of ST with bicarbonate is extremely fast and is a prerequisite for metal uptake (eqs 1 and 2, refs *5* and *35*).

$$H_2T'_N\text{-}T'_CH_2 + HCO_3^- \rightleftharpoons H_2T'_N\text{-}T_C\,H_3 \text{ (very fast)} \quad (1)$$

$$H_2T'_N\text{-}T_CH_3 + HCO_3^- \rightleftharpoons T \text{ (very fast)} \quad (2)$$

$H_2T'_N\text{-}T'_CH_2$ is the protein not interacting with bicarbonate,

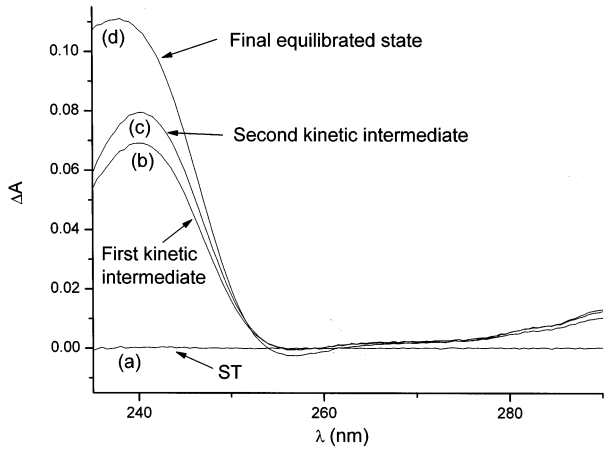

FIGURE 2: Differential absorption spectra of (a) ST (4.70 μM), (b) 200 and 250 s, (c) 2500 and 3000 s, and (d) 20 h after the addition of aluminum citrate (0.25 mM) with $[HCO_3^-] = 20$ mM at pH 8.22, $\mu = 0.2$ and 25 ± 0.5 °C.

$H_2T'_N$-T_CH_3 is the protein of which only the C-site is interacting with bicarbonate that from now on will be represented as T_CH_3, and T is the protein in an unknown state for the C-site $K_{Cbic} = [H_2T'_N\text{-}T'_CH_2][HCO_3^-]/[T_CH_3] = 4.3$ mM and for the N-site $K_{Nbic} = [H_2T'_N\text{-}T_CH_3][HCO_3^-]/[T] = 36$ mM (*35*). Moreover, it should be noted that under our experimental conditions (10 mM $\leq [HCO_3^-] \leq$ 30 mM), only 10−40% of the C-site of ST and 1−4% of that of the N-site are interacting with bicarbonate (*35*).

These kinetic observations and the fact that in the presence of one aluminum equivalent only the C-site of the transferrin becomes metal-loaded (*34*) imply that, as with iron (*29*), complex formation between Al(III) and ST primary takes place on one of the two sites of the protein. This metal uptake can proceed by three possible paths (*28*). In the first, the fastest step in Figure 1 is the formation of a ternary complex between ST and aluminum monocitrate. At constant pH and bicarbonate values, we can to a rough approximation write eq 3 (*28*).

$$T + AlL \underset{k_{-1obs}}{\overset{k_{1obs}}{\rightleftharpoons}} TAlL \quad (3)$$

with TAlL as the ternary kinetic intermediate in an unknown state of protonation; k_{1obs} and k_{-1obs} are the observed kinetic constants at fixed pH and $[HCO_3^-]$.

Eq 3 can be accompanied by one or several proton losses. However, since our experiments are performed in a buffer at a fixed pH value, we can write eq 4 (*28*).

$$(\tau'_1)^{-1} = k_{1obs}([T] + [AlL]) + k_{-1obs} \quad (4)$$

To respect the chemical relaxation approximation, our experimental conditions were set so as $c_2 \gg c_1$ (*26*). Therefore, eq 4 can be expressed as eq 5.

$$(\tau'_1)^{-1} = k_{1obs}(c_2) + k_{-1obs} \quad (5)$$

At fixed pH and $[HCO_3^-]$, the first kinetic process of Figure 2 depends on c_1 and c_2, whereas eq 5 is only dependent on c_2. Subsequently, eq 3 is discarded.

In the second possibility, metal exchange between the chelate and the protein occurs after chelate dissociation. We can, at fixed pH and $[HCO_3^-]$, write to a rough approximation eqs 6 and 7 (*28*).

$$Al^{3+} + L^{3-} \underset{k_{-AlL}}{\overset{k_{AlL}}{\rightleftharpoons}} AlL \quad (6)$$

$$Al^{3+} + T \underset{k_{-2obs}}{\overset{k_{2obs}}{\rightleftharpoons}} TAl \quad (7)$$

with $K_{AlL} = [Al^{3+}][L^{3-}]/[AlL]$, $K'_1 = [Al^{3+}][T]/[TAl]$, and TAl is the kinetic intermediate.

The reciprocal relaxation times associated with eqs 6 and 7, when each in turn is assumed rate-limiting, are expressed as eqs 8 and 9, respectively (Appendix).

$$(\tau'_1)^{-1} = k_{-AlL} + k_{AlL}\{[Al^{3+}] + [L^{3-}](K'_1 + [Al^{3+}])/(K'_1 + [Al^{3+}] + [T])\} \quad (8)$$

$$(\tau'_1)^{-1} = k_{-2obs} + k_{2obs}\{[Al^{3+}] + [T](K_{AlL} + [Al^{3+}])/(K_{AlL} + [Al^{3+}] + [L^{3-}])\} \quad (9)$$

Eqs 8 and 9 do not depend on the aluminum chelate concentration ($[AlL] \approx c_2$). Subsequently, eqs 6 and 7 were discarded.

In the last possibility, we shall assume that the first step in aluminum uptake occurs by a reaction similar to that reported for iron exchange between an iron chelate and the protein (*27*, *29*). At fixed pH and $[HCO_3^-]$, this can be approximatively estimated by eq 10.

$$T + AlL \underset{k'_{-obs}}{\overset{k'_{obs}}{\rightleftharpoons}} TAl + L^{3-} \quad (10)$$

The reciprocal relaxation time equation associated with eq 10 can be expressed as eq 11 (*24*, *25*, *29*).

$$\tau_1^{-1} = k'_{obs}([T] + [AlL]) + k'_{-obs}([TAl] + [L^{3-}]) \quad (11)$$

Under our experimental conditions where $c_2 > c_1$ and no citrate anion added, eq 10 can be expressed as eq 12 (*29*).

$$\tau_1^{-1} \approx k'_{obs}c_2 + k'_{-obs}2c_1 \quad (12)$$

At 5 fixed pH, $[HCO_3^-]$, and c_1 values, eq 12 is respected as shown by the linear least-squares regression of τ_1^{-1}against c_2 (Figure 3). This implies that the first step in aluminum uptake by ST is a metal exchange between the chelate and the protein.

The dependence of the experimental reciprocal relaxation times related to the first step of Figure 2 on pH and $[HCO_3^-]$ leads us to assume that the exchange of Al(III) between the aluminum chelate involves, as in the case of iron (*27*), one or several proton dissociations. This can be expressed by eqs 13 and 14 (*5*).

$$T_CH_3 + AlL \underset{k_{-1}}{\overset{k_1}{\rightleftharpoons}} T_CH_3Al + L^{3-} \text{ (rate-limiting)} \quad (13)$$

$$T_CH_3Al \rightleftharpoons T_CH_{3-m}Al + mH^+ \text{ (fast)} \quad (14)$$

where m is the number of protons lost in eq 14, $K_1 = [T_CH_3$

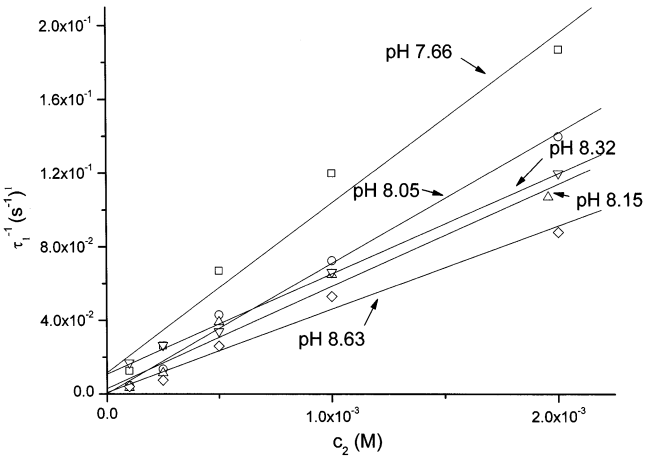

FIGURE 3: Plot of $(\tau_1)^{-1}$ against c_2 at five fixed pH values and 25 °C with $[HCO_3^-] = 20$ mM, $c_1 = 4.1$ μM, and $\mu = 0.2$, pH 7.66. Intercept, $(1.1 \pm 0.2) \times 10^{-2}$ s^{-1}; slope, 90 ± 15 M^{-1} s^{-1}, $r = 0.98631$; pH = 8.05. Intercept, $(2 \pm 7) \times 10^4$ s^{-1}; slope, 71 ± 7 M^{-1} s^{-1}; $r = 0.99638$; pH = 8.15. Intercept, $(3.0 \pm 0.1) \times 10^{-3}$ s^{-1}; intercept, 55 ± 10 M^{-1} s^{-1}; $r = 0.98868$; pH = 8.32. Intercept, $(1.1 \pm 0.1) \times 10^2$ M^{-1} s^{-1}; slope, 55 ± 2 s^{-1}; $r = 0.99841$; pH = 8.63. Intercept, $(8 \pm 10) \times 10^{-4}$ s^{-1}; slope, 45 ± 7 M^{-1} s^{-1}; $r = 0.99095$.

Al][L]/[T_CH_3][AlL], and $K_{1a} = [H^+]^m[T_CH_{3-m}Al]/[T_CH_3Al]$. The reciprocal relaxation time associated with rate-limiting eq 13 is expressed as eq 15 (*5*).

$$\tau_1^{-1} = k_{-1}\{(1 + [H^+]^m/K_{1a})[T_CH_3Al] + [L^{3-}][H^+]^m/K_{1a}\} + k_1\{(c_2 - c_1)/\gamma + [T_CH_3]\}(1 + [H^+]^m/K_{1a}) \quad (15)$$

with $\gamma = (1 + K_{bic}/[HCO_3^-])$.

Under our experimental conditions where $c_2 \geq 10\ c_1$, $[L^{3-}] \approx c_1$ and since $[T_CH_3Al] = c_1/(1 + K_{1a}/[H^+]^m)$ eq 15 can be expressed as eq 16.

$$\tau_1^{-1}/([H^+]^m 2c_1) \approx k_{-1}/K_{1a} + k_1 c_2(1 + [H^+]^m/K_{1a})/([H^+]^m \gamma 2c_1) \quad (16)$$

At fixed pH and $[HCO_3^-]$, in the absence of any analytical concentration of citrate and at constant c_1, eq 16 can be expressed as eq 17.

$$\tau_1^{-1}/[H^+]^m = k_{-1}(2c_1/K_{1a}) + k_{obs}c_2 \quad (17)$$

in which

$$k_{obs}\gamma = k_1/[H^+]^m + k_1/K_{1a} \quad (18)$$

Five k_{obs} values were determined from the slope of the five regression lines of Figure 3 as follows: $k_{obs} = k'_{obs}/(2c_1[H^+]^m)$. A good linear regression of the k_{obs} against eq 18 was only obtained for $m = 1$ (Figure 4). From the slope and intercept of the best line, we determined $k_1 = 47 \pm 3$ M^{-1} s^{-1} and $K_{1a} = 15 \pm 3$ nM. This last value is within the experimental uncertainty equal to that reported for the same proton loss during iron exchange with two different iron chelates, nitrilotriacetate and acetatohydroxamate (*27*, *29*). K_{1a} being known, a linear regression of all experimental data at different pH, c_1, c_2, and $[HCO_3^-]$ values against eq 16 was obtained (Figure 5). $k_1 = 45 \pm 3$ M^{-1} s^{-1} was confirmed within the experimental uncertainty, and $k_{-1}/K_{1a} = (1.5 \pm 0.5)$ 10^{11} s^{-1} was determined from the slope and intercept of the best regression line of Figure 5. This allowed the measurement of $K_1 = k_1/k_{-1} = (2.0 \pm 0.6) \times 10^{-2}$.

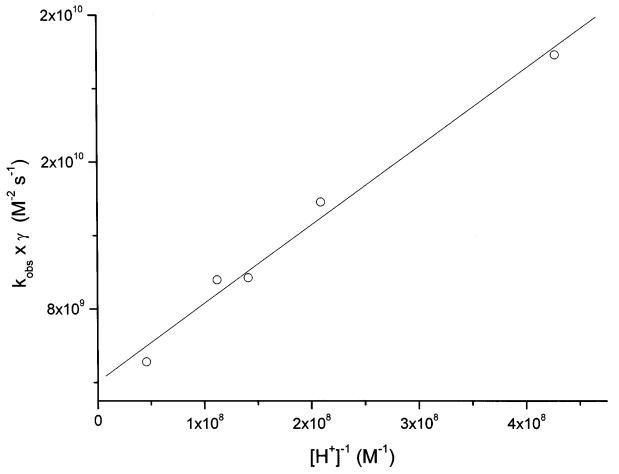

FIGURE 4: Plot of $k_{obs}\gamma$ against $1/[H^+]$. Intercept, $(3.0 \pm 0.5) \times 10^9$ M^{-2} s^{-1}; slope, 47 ± 3 M^{-1} s^{-1}; $r = 0.99591$.

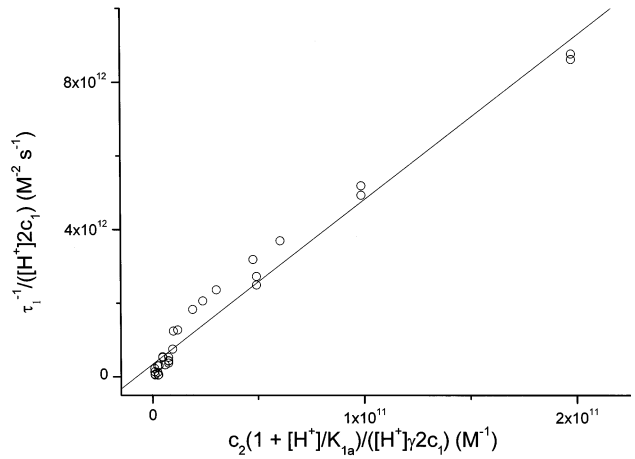

FIGURE 5: Plot of $\tau_1^{-1}/([H^+]2c_1)$ against $c_2(1 + [H^+]/K_{1a})/([H^+]\gamma 2c_1)$ with $1\ \mu M \leq c_1 \leq 6\ \mu M$; $20\ mM \leq [HCO_3^-] \leq 50$ mM; $7.60 \leq pH \leq 8.80$; and $0.1\ mM \leq c_2 \leq 1.5$ mM at 25 °C and $\mu = 0.2$. Intercept, $(1.5 \pm 0.5) \times 10^{11}$ s^{-1}; slope, 45 ± 3 M^{-1} s^{-1}; $r = 0.98839$.

Second Kinetic Process. In the second kinetic process of Figure 1, the first kinetic intermediate T_CH_2Al yields the second kinetic intermediate (Figure 2). The experimental reciprocal relaxation times associated with this second kinetic process of Figure 1b (τ_2^{-1}) depend only on pH, as observed for the first change in conformation following the uptake of iron by ST (*27*, *29*). We, therefore, were tempted to ascribe this second process to rate-limiting eq 19 in which T_CH_2Al undergoes a modification in conformation followed by l diffusion-controlled proton losses (*5*).

$$T_CH_2Al \underset{k_{-2}}{\overset{k_2}{\rightleftharpoons}} T'_CH_2Al \quad (19)$$

$$T'_CH_{2-l}Al + lH^+ \rightleftharpoons T'_CH_2Al \quad (20)$$

where T'_CH_2Al is the second kinetic intermediate with $K_{2a} = [T'_CH_{2-l}Al][H^+]^l/[T'_CH_2Al]$.

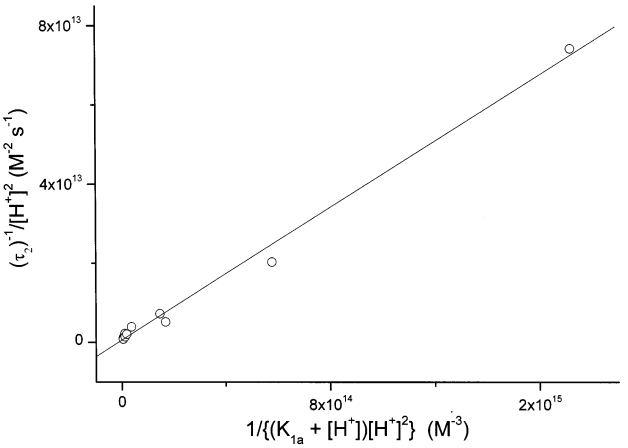

FIGURE 6: Plot of $(\tau_2)^{-1}/[H^+]^2$ against $k_2K_{1a}/\{(K_{1a} + [H^+])[H^+]^2\}$ with $1\mu M \leq c_1 \leq 6\ \mu M$; 0.1 mM $\leq c_2 \leq$ 1.5 mM; and 10 mM $\leq [HCO_3^-] \leq$ 30 mM at 25 °C and $\mu = 0.2$. Intercept, $(6.05 \pm 12) \times 10^{11}$ M^{-1} s^{-1}; slope, $(4.2 \pm 0.2) \times 10^{-2}$ s^{-1}; $r = 0.99626$.

The reciprocal relaxation time equation associated with rate-limiting eq 19 can be expressed as (*5*)

$$(\tau_2)^{-1}/[H^+]^l = k_2K_{1a}/\{(K_{1a} + [H^+])[H^+]^l\} + k_{-2}/K_{2a} \quad (21)$$

A good linear regression of the data against eq 21 was only obtained for $l = 2$ (Figure 6). $k_2 = (4.20 \pm 0.02) \times 10^{-2}$ s^{-1} was determined from the slope of the best regression line. This k_2 value is 2 orders of magnitude lower than that determined for the uptake of iron. The uncertainty on the intercept was too high to allow any measurement of k_{-2}/K_{2a}. Ascribing the second kinetic phenomenon to a pure proton loss or to a proton loss preceding a modification in the conformation of the first kinetic intermediate was not supported by the experimental data (*29*). The second modification in conformation of the protein is, therefore, accompanied by two proton losses.

Third Kinetic Process. In the third kinetic process of Figure 1c, the second kinetic intermediate yields the final thermodynamic aluminum-loaded ST species (Figure 2). This final process is extremely slow and occurs with reciprocal experimental relaxation time $\tau_3^{-1} = (6 \pm 2) \times 10^{-5}$ s^{-1}. It does not seem to depend on any of the experimental parameters (pH, c_1, and c_2). It occurs in about 20 h whether the protein reacts with 1 or 2 aluminum equiv. It does not occur when the C-site of the protein is already metal-loaded (iron or aluminum) in its thermodynamic state of equilibrium. It, therefore, rate-controls the uptake of a second aluminum by the ST. Furthermore, the fact that the measured τ_3^{-1} are independent of the concentrations of the species present in the medium indicates that within the experimental uncertainties, this final kinetic process is associated with a monomolecular reaction such as a change in conformation (*24*, *25*). Therefore, we shall associate the slow kinetic process of Figure 1c with a final change in the conformation of ST during which the metal-loaded protein attains its final state of equilibrium. Proton losses can accompany this process. Nonetheless, they cannot be detected at this stage.

Interaction of Metal-Loaded ST with TFR. TFR possesses an intrinsic fluorescence spectrum for an excitation wavelength of $\lambda_{ex} = 280$ nm. In aqueous media with $\mu = 0.2$ and pH = 7.40, TFR is in an aggregate form (*22*). In the presence of 1% CHAPS, TFR becomes monomolecular (*22*). The differences in the emission spectra of the transferrin species and that of TFR will allow us to determine the dissociation constants involved in the interaction of the metal-loaded transferrin species with receptor 1 (Figure 7). The presence of the CHAPS detergent manifests by a bathochromic shift of the emission maximum of the protein spectra that, thus, differs from those already reported for transferrins in detergent-free aqueous media (*27*, *35*).

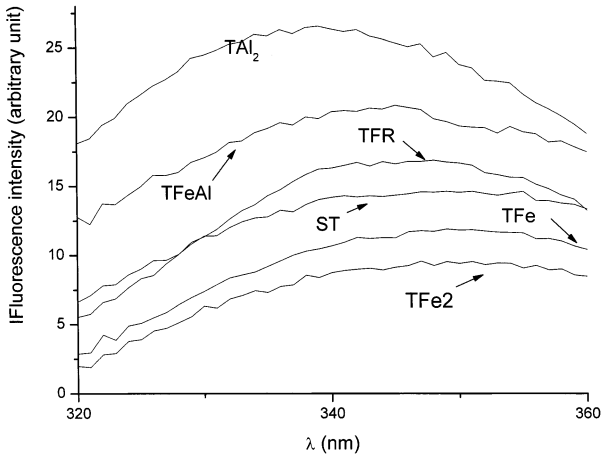

FIGURE 7: Fluorescence emission spectra of the different metal-free or metal-loaded ST species after subtraction of the emission contribution of the solvent. All spectra are reported for an excitation wavelength $\lambda_{ex} = 280$ nm for protein species concentrations of 5 nM in the presence of 1% CHAPS at pH 7.45, $\mu = 0.2$ M, and 25 °C.

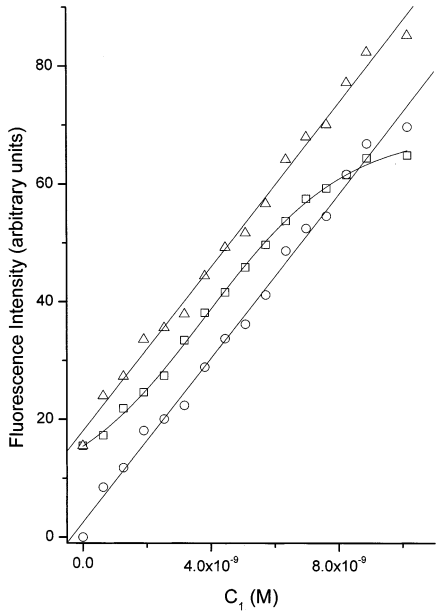

FIGURE 8: Variation with c_1 of fluorescence emission after subtraction of the emission contribution of the buffer of (○) TFe_2, (□) TFe_2 in the presence of TFR, and (△) that of the theoretical sum of the fluorescence emission contributions of TFe_2 and TFR at $\lambda_{em} = 337$ nm for an excitation wavelength $\lambda_{ex} = 280$ nm with $c_4 = 4.8$ nM, $0 \leq c_1 \leq 10$ nM in the presence of 1% CHAPS at pH 7.46, $\mu = 0.2$, and 25 ± 0.5 °C.

Iron-Loaded ST and TFR. Adding ST to TFR in the presence or absence of 1% CHAPS leads to a shift in the emission maximum wavelength that is accompanied by a modification in the fluorescence emission (Figure 8). We associate this fluorescence variation with the molecular

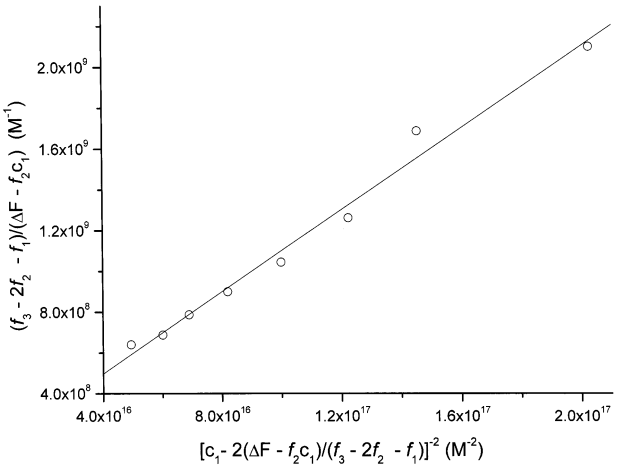

FIGURE 9: Plot for TFe_2 of $(f_3 - 2f_2 - f_1)/(\Delta F - f_2c_1)$ against $[c_1 - 2(\Delta F - f_2c_1)/(f_3 - 2f_2 - f_1)]^{-2}$ with $c_4 = 4.8$ nM, 2 nM $\leq c_1 \leq$ 10 nM, CHAPS 1%, and $[HCO_3^-] = 20$ mM at pH 7.46, $\mu = 0.2$, and 25 ± 0.5 °C. Intercept, $(1 \pm 1) \times 10^8$ M^{-1}; slope, $(1.0 \pm 0.1) \times 10^{-8}$ M^{-2}; $r = 0.99241$.

interaction of the receptor with iron-loaded ST. Similar spectral modifications are also observed with a ST only the C-site of which is iron-loaded, and no spectral change is observed with apo-ST. This variation in the fluorescence emission (Figure 8) implies, as expected, the existence of an interaction between the receptor and the iron-loaded ST.

The TFR homodimer possesses two interaction sites each of which binds an iron-loaded transferrin (TFe_2) (*36*, *37*).

$$TFR + 2TFe_2 \rightleftharpoons TFR{-}(TFe_2)_2 \qquad (22)$$

with TFe_2 as the iron-saturated ST in neutral media in an unknown state of protonation and charge, $TFR{-}TFe_2$, the holo-ST TFR adduct, and $K = [TFR][TFe_2]^2/[TFR{-}(TFe_2)_2]$.

The variations in $TFR{-}(TFe_2)_2$ concentrations and in fluorescence emission intensity obey eq 23 (Appendix)

$$(f_3 - 2f_2 - f_1)/(\Delta F - f_2c_1) = 1/c_4 + K/\{c_4[c_1 - 2(\Delta F - f_2c_1)/(f_3 - 2f_2 - f_1)]^2\} \qquad (23)$$

in which f_1, f_2, and f_3 are the experimental proportionality factors linking the fluorescence emission to [TFR], $[TFe_2]$, and $[TFR{-}(TFe_2)_2]$; c_4 is the TFR concentration; F_0 is the fluorescence intensity of TFR in the absence of transferrin; and F isthe fluorescence intensity with $\Delta F = F - F_0$. Figure 9 shows a linear least-squares regression of the data against eq 23 for the iron-saturated ST in the presence of 1% CHAPS at 25 °C. Other linear regressions were obtained at 25 and 37 °C for the iron-saturated ST and for the only C-site iron-loaded ST in the presence and absence of CHAPS. From the slopes of the best regression lines, eight K values were determined. From these K values average dissociation constants $K^{1/2} = K_{av}$ were also determined (Figure 9). The limits of uncertainty did not allow us to make a distinction between the values of the dissociation constants measured at 25 °C and those measured at 37 °C (Table 1). The K_{av} related to the interaction of TFR with TFe_2 are about 2−5-fold higher than those reported by other techniques with labeled proteins (*36*, *37*). As for those related to the interaction with FeT, they were not known before this work. No interaction was observed with apo-ST and TFR, confirming the latter lack of affinity for TFR (*36*, *37*).

Table 1: Average Stability Constants of the Interaction of Iron-Loaded ST with TFR in the Absence and Presence of 1% CHAPS at pH 7.47 and $\mu = 0.2$ at 25 ± 0.5 °C or 37 ± 0.5 °C

state of iron load	K_{av} in the absence of CHAPS (nM)	K_{av} in the presence of 1% CHAPS (nM)
iron-saturated	6.0 ± 0.6	7.0 ± 0.7
C-site iron-loaded	3 ± 1	5 ± 1

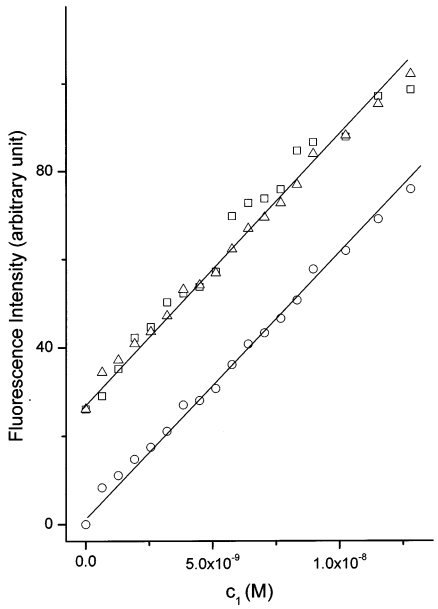

FIGURE 10: Variation of the fluorescence intensity after subtraction of that of the buffer with c_1 at $\lambda_{em} = 337$ nm for an excitation wavelength $\lambda_{ex} = 280$ nm of (○) TAl_2, (□) TAl_2 in the presence of TFR, and (△) that of the sum of the fluorescence emission contributions of TAl_2 and TFR with $c_4 = 4.8$ nM, $0 \leq c_1 \leq 15$ nM in the presence of 1% CHAPS at pH 7.46, $\mu = 0.2$, and 25 ± 0.5 °C.

Interaction of Aluminum-Loaded ST with TFR. When Al(III)-saturated transferrin (Al_2ST) and the mixed C-site iron-loaded/N-site aluminum-loaded ST (FeTAl) are incubated with TFR, the observed emission spectra are always the exact sum of the contributions of the free Al_2ST or FeTAl and TFR (Figure 10). The same spectra are still observed after several hours of incubation at 25 or 37 °C. To achieve a better understanding of this undetected interaction, size-exclusion chromatography was performed with columns of Sephadex G100 Super Fine. This matrix possesses a fractionation range of 50−100 kDa. It was, therefore, expected to retain the metal-loaded transferrin (~80 kDa) and exclude TFR (~190 kDa) or TFR in interaction with Fe_2ST or Al_2-ST (~270 kDa). Five chromatography experiments were performed with TRF, Fe_2ST, Al_2ST, and two mixtures of TFR and Fe_2ST or Al_2ST at identical concentrations. The results are summarized in Table 2 where the highest absorption detected at 280 nm is normalized as 1 when TFR is involved and as 0.5 with metal-loaded transferrins in the absence of the receptor. This is because at 280 nm, the molecular extinction coefficient we measured for the receptor (215 000 M^{-1} cm^{-1}) is about 2-fold that of the metal-loaded transferrins (95 000 M^{-1} cm^{-1}). Metal-loaded transferrins were both eluted as a single species in the eighth to ninth fraction just after the full elution volume (Table 2). TFR and the mixture of TFR and Fe_2ST were eluted as a single species in the third fraction just after the void volume (Table

Table 2: Relative Absorption of Fractions of 400 μL Eluted on Sephadex G100 Super Fine 2 mL Columns with Deposited Volumes of 100 μL of 1 μM Fe_2ST, Al_2ST, TFR, and an Equimolar Mixture of Fe_2ST or Al_2ST with TFR

protein	A_{norm}[a] 400 μL	A_{norm} 800 μL	A_{norm} 1200 μL	A_{norm} 1600 μL	A_{norm} 2000 μL	A_{norm} 2400 μL	A_{norm} 2800 μL	A_{norm} 3200 μL	A_{norm} 3600 μL	A_{norm} 4000 μL
Fe_2ST or Al_2ST	0.01	0.05	0.03	0.02	0.02	0.03	0.02	0.1	0.5[b]	0.03
TFR	0.02	0.02	1[c]	0.05	0.05	0	0.03	0.02	0.02	0.02
Fe_2ST/TFR	0.01	0	1	0.1	0.06	0.04	0.02	0.03	0.01	0.01
Al_2ST/TFR	0.04	0.02	1	0.1	0.1	0.05	0.05	0.4	0.2	0.04

[a] A_{norm} is the relative absorption at 280 nm of each elution fraction when the highest absorption is normalized as 0.5[b] for metal-loaded transferrins in the absence of the receptor and as 1[c] for metal-loaded transferrins in the presence of the receptor.

2). As for the presumed TFR−Al_2ST adduct, it was eluted in two main fractions with the first part in the third, the second in the eighth, and a smaller part in the ninth fraction (Table 2). The first fraction contained essentially TFR, and the last two fractions contained essentially receptor-free transferrin. Therefore, the Al_2ST−TFR adduct behaves as a mixture of the two protein species or dissociates on the chromatography column. All protein concentrations were spectrophotometrically checked and corresponded after elution to the expected values. Since no measurable molecular interaction between TFR and Al_2ST or FeTAl is detected either by fluorescence spectroscopy or by size-exclusion chromatography, the affinity of the aluminum-saturated ST for TFR must be much lower than that of the iron-loaded species.

DISCUSSION

Aluminum uptake by ST was once assumed to first occur by the N-site (*38*). Nonetheless, the affinity of the C-site for aluminum is higher than that of the N-site; the order of lobe loading by aluminum is identical to that of iron, which first occurs with the C-site. ST was isolated with its C-site loaded with aluminum and its N-site aluminum-free, and to the best of our knowledge, was never isolated the other way around (*7*, *11*, *34*, *39*). In addition, aluminum uptake by the N-site of a C-site iron-loaded transferrin in its final state of equilibrium is identical to that of a second aluminum uptake by a ST having reacted for 24 h with 1 equiv of AlL. In both cases, the final process of Figure 1 is not observed. This implies that the second iron and aluminum uptakes occur on the same site, which in the case of monoferric transferrin is the N-site. Furthermore, the exchange of aluminum between the chelate and the ST depends on the interaction of [HCO_3^-] with the C-site (eqs 1 and 13). This implies a prior interaction of the site with bicarbonate (Table 2, eq 1). Under our experimental conditions, only the C-site of ST interacts with bicarbonate (*35*). We, therefore, assumed that aluminum uptake starts with this C-site in interaction with bicarbonate. However, even if aluminum uptake started with the N-site, the general mechanism of aluminum exchange between AlL and ST, added to the conclusions drawn in this work, would apply as well.

In Table 3, we summarize the mechanism of aluminum uptake by ST and compare it to that of iron. Fe(III) uptake by ST occurs by four identified kinetic steps (*27*, *29*). With aluminum, we only observe three kinetic processes. This does not imply that aluminum uptake by ST proceeds only by the three steps of Figure 1. Other steps undetected by our spectrophotometric techniques may be involved. In both mechanisms of aluminum and iron uptake, the first detected step is always that of a metal exchange between a chelate and the C-site of ST in interaction with bicarbonate (Table 3; eqs 1, 3, and 25). These two processes are followed by a single proton loss occurring with the same pK_a for both iron and aluminum ST complexes (Table 3, eqs 4 and 26). However, this does not imply that the two mechanisms of Table 3 are similar. In the case of iron, the metal chelates were nitrilotriacetate and acetylhydroxamate, whereas with aluminum we used the monocitrate chelate. Both acetylhydroxamato-iron(III) and nitrilitriacetato-iron(III) dissociate very rapidly and do not rate-control the metal uptake by the protein (*27*). Iron uptake from the ferric citrate is extremely slow and was not reported in Table 3 (*40*). Indeed, with this chelate, iron uptake is under the kinetic control of the very slow dissociations of ferric citrate and its polymer (*27*, *40*). In contrast, aluminum citrate dissociates more rapidly than the first step of the metal uptake by ST (*41*, *42*). Aluminum citrate dissociation does not, therefore, rate-control aluminum exchange with ST. Moreover, the choice of aluminum monocitrate as a metal-donating chelate was dictated by the fact that citrate is considered along with transferrin as a potential aluminum transport agent in biological fluids (*10*).

The same ligands (2 Tyr, 1 His, and 1 Asp) are engaged in complex formation between ST and iron or aluminum (*3*, *4*, *33*, *34*, *39*). This, however, does not imply that the two final metal-loaded species have identical structures or conformations. Unfortunately, very little structural information about the aluminum−ST complex is available (*7*, *33*, *34*, *39*).

Aluminum uptake first occurs by the C-site and is then followed by that at the N-site. The final slow step of Figure 1c occurs whether the protein reacts with one or more than one metal equivalent. With more than one metal equivalent, this slow process rate-controls the uptake of the metal by the N-site (Table 3, eqs 22 and 23). With one metal equivalent, the slow process allows the protein to attain a state of equilibrium in which only the C-site becomes metal-loaded, and the N-site becomes capable of reacting with another metal in a fashion identical to that of the C-site. This was also established for iron uptake (Table 3, eq 33). This implies, as in the case of iron, the existence of cooperativity between the sites toward aluminum uptake, which signifies that the N-site of the protein cannot acquire any metal unless the C-site is already metal-loaded. Moreover, this cooperativity can explain why the N-site of a C-site iron-loaded or aluminum-loaded protein in its thermodynamic state of equilibrium becomes capable of acquiring another aluminum by paths similar to those observed for the C-site of an apoprotein (Table 3, eqs 22 and 23).

Table 3: General Mechanisms of Aluminum and Iron (*27*) Uptake by ST

reaction		average direct rate constant	average reverse rate constant	equilibrium constant
$T'_CH_2 + HCO_3^- \rightleftharpoons T_CH_3$	(1)			4.35 mM
		Aluminum uptake		
$T_CH_3 + AlL \rightleftharpoons T_CH_3Al + L$	(3)	$(44 \pm 3)\ M^{-1}\ s^{-1}$	$(2.3 \pm 0.6) \times 10^3\ M^{-1}\ s^{-1}$	$(2.0 \pm 0.6) \times 10^{-2}$
$T_C\ H_3Al \rightleftharpoons T_CH_2Al + H^+$	(4)			(15.0 ± 3) nM
$H_jT_NT_CH_2Al \rightleftharpoons TH_{j+2}Al$[a]	(19)	$(4.20 \pm 0.02) \times 10^{-2}\ s^{-1}$		
$TH_jAl + 2H^+ \rightleftharpoons TH_jAl$	(20)			
$TH_jAl \rightleftharpoons T'H_jAl$	(21)			
$T'H_jAl + AlL \rightleftharpoons L + T'H_jAl_2$	(22)			
$T'H_jAl_2 \rightleftharpoons T''H_jAl_2$	(23)			
$T_CH_3 + Al^{3+} \rightleftharpoons T_CH_3Al$	(24)[c]			~35 nM
		Iron uptake		
$T_CH_3 + FeL' \rightleftharpoons T_CH_3Fe + L'$	(25)	$8.0 \times 10^4\ M^{-1}\ s^{-1}$	$7.5 \times 10^4\ M^{-1}\ s^{-1}$	1.00
$T_CH_3Fe \rightleftharpoons T_CH_2Fe + H^+$	(26)			16 nM
$H_3T_NT_CH_2Fe \rightleftharpoons TH_5Fe$	(27)	$2.80\ s^{-1}$		
$TH_5Fe \rightleftharpoons TH_{(5-l)}Fe + lH^+$[b]	(28)			
$T'H_{(5-l)}Fe \rightleftharpoons TH_{(5-l)}Fe$	(29)	$6.2 \times 10^{-2}\ s^{-1}$		
$T'H_{(4-l)}Fe + H^+ \rightleftharpoons T'H_{(5-l)}Fe$	(30)			6.8 nM
$T'H_{(4-l)}Fe \rightleftharpoons T''H_{(4-l)}Fe$	(31)			
$T'H_{(4-l)}Fe_2 \rightleftharpoons T''H_{(4-l)}Fe_2$	(32)			
$T'H_{(4-l)}Fe + \rightleftharpoons L + T'H_{(4-l)}Fe_2$	(33)			
$T_CH_3 + Fe^{3+} \rightleftharpoons T_CH_3Fe$	(34)[c]			$\sim 1 \times 10^{-16}$ M

[a] j is unknown. [b] $l = 2$ or 3 (*27*). [c] Reactions 24 and 34 are written to introduce equilibrium constants independent of the ligand nature.

The affinity of the C-site of ST for aluminum at the end of the first metal exchange $\beta_1 = [T_CH_3Al]/[T_CH_3][Al^{3+}]$ (Table 3, eq 24) can be determined from $\beta_{Alcit} = [AlL]/[Al^{3+}][L^{3-}] = 1 \times 10^8\ M^{-1}$ (*23*) and K_1 as $\beta_1 = \beta_{Alcit}/K_1 = (2.2 \pm 1.0) \times 10^6\ M^{-1}$. β_1 is lower than β_{Alcit}. It is, moreover, lower by about 10 orders of magnitude than that determined for iron ($\sim 1 \times 10^{16}\ M^{-1}$) at the same stage (Table 3). Aluminum exchange is accompanied by a proton loss ($K_{1a} = 15$ nM; Table 3, eq 4). Complex formation occurs between Al(III) and the carboxylate of the aspartate, the imidazole of histidine, and the phenolates of the two tyrosines (*34*). In the classical open-conformation model of the apoprotein, these protein ligands are in direct contact with the outside medium (*3*, *4*). In this case, the ligand pK'_as is assumed to be close to those in water, p$K'_a \approx 10$ for the tyrosine phenolate (*6*, *30*). When a metallic complex forms, the apparent pK'_a of the ligand can decrease by ΔpK_a. The higher this ΔpK_a is, the higher the affinity of the ligand for the metal becomes (*43*). Therefore, in the case of the ST, the affinity of the site for aluminum at the end of eq 3 (Table 3) after the proton loss would be $\beta = \beta_1 K_{1a}/K'_a \approx 1 \times 10^8\ M^{-1}$ (*43*). With iron, the first proton loss after metal uptake occurs with the same p$K_a = 7.80$ (Table 3, eqs 4 and 26), and the affinity value at the end of this proton dissociation is about $10^{18}\ M^{-1}$. Consequently, no competition can be possible between aluminum and iron toward metal uptake by ST. Aluminum can, therefore, only react with the available apo- or monoferric transferrins. Moreover, β is very close to the affinity of the citrate anion for aluminum in neutral media (*23*). Subsequently, at the end of eq 3 and before the slow modification in conformation of Figure 2, aluminum is distributed between transferrin and citrate. At the end of this first kinetic step, the C-site aluminum-loaded protein undergoes a new change in conformation accompanied by the loss of two protons (Table 3, eqs 19 and 20). As with iron, the conformation of the protein is believed to transit from the open apo-form to the closed metal-loaded protein (*34*). The overall affinity of ST for aluminum was reported to be in the 10^{12} (N-site) to $10^{13}\ M^{-1}$ (C-site) range (*7*). This is 4 orders of magnitude higher than β_{Alcit} and implies that at final equilibrium the distribution of aluminum between citrate and ST is largely in favor of ST. However, if aluminum transport in a living species occurs more rapidly than the second and third steps of Figures 2 and 4, the affinities involved in the uptake of aluminum would then be those prevailing at the end of partial equilibria 3 and 9 (β and β_1). These are 4 or 5 orders of magnitude lower than those reported at thermodynamic equilibrium (*7*).

The dissociation constants associated with the interactions of the only C-site iron-loaded and the iron-saturated ST with TFR (Table 1) constitute, to the best of our knowledge, the first direct data obtained with the native unlabeled proteins. These constants are of about 2−5-fold higher than those reported in the literature in vitro with the labeled proteins (Table 1) (*36*, *37*). They, moreover, show that the affinity of TFR for the only C-site iron-loaded ST is a little higher than that for the iron-saturated protein.

The most unexpected result is that we do not observe in the concentration range used in this work any interaction between TFR and aluminum-saturated or C-site iron-loaded/N-site aluminum-loaded transferrin. In some cell lines and in cell extracts, reports estimated that the affinity of the aluminum-loaded ST for TFR is of the same order of magnitude as that of the iron-loaded protein (*13*, *44*). However, ST interacts with two specific receptors, TFR and receptor 2 (*45*), and our experiments were performed in vitro with receptor 1. Although improbable at least for the mixed iron and aluminum protein complex, the interaction of TFR with the aluminum-loaded ST may not be accompanied by the emission spectra variations observed with iron-loaded ST. In this case, it would have been eluted from the size exclusion chromatography column as a single protein as with the Fe_2ST−TFR adduct and not as the protein mixture of Table 2. If we assume that one of the steps in the interaction of the transferrin with its receptor is based on a structural recognition (*46*), such as for example a docking process, we

will have to consider that the presence of aluminum modifies the conformation of the protein in such a way that this structural identification becomes less efficient. This modification can be slight but sufficient to inhibit the interaction between the two proteins. All this is, of course, speculative, and more data are required about the mechanism of interaction of ST with TFR and about the structure of the adduct formed.

Aluminum is believed to use the transferrin receptor-mediated pathway to be transported from the biological fluids to the brain or other organs (*10*, *12*, *13*, *19*, *44*). Part of the toxicity of aluminum may, thus, be explained by the fact that its transport competes with that of iron, which disturbs its metabolism in the cell (*12*, *13*). This explanation is very attractive, although it cannot answer the question of whether aluminum transport occurs by the iron-acquisition pathway. Our data indicate that the affinity of the transferrin receptor 1 for the aluminum−transferrin complex is much too weak to be detected. They, however, cannot be directly transposed in vivo and do not imply that aluminum transport in a living species cannot occur by TFR mediated endocytosis. We should, nevertheless, keep in mind that the transferrin-mediated iron acquisition pathway is one of many metal transport systems that prevail in a living organism (*47*, *48*). Some divalent metals, such as Cu(II), Zn(II), or Cr(II), are known to form stable complexes with transferrins without using the transferrin-mediated iron acquisition path (*47*−*53*). Hence, aluminum may also use paths other than that of iron to reach its targets inside the cellular medium.

APPENDIX

The reciprocal relaxation time equations are derived by the substitution methods (*24*, *25*). The rate equations associated with eqs 6 and 7 when each is considered rate-limiting can be expressed as eqs 35 and 36, respectively.

$$-\mathrm{d}\Delta[\mathrm{AlL}]/\mathrm{d}t = k_{-\mathrm{AlL}}\Delta[\mathrm{AlL}] - k_{\mathrm{AlL}}([\mathrm{L}^{3-}]\Delta[\mathrm{Al}^{3+}] + [\mathrm{Al}^{3+}]\Delta[\mathrm{L}^{3-}]) \quad (35)$$

$$-\mathrm{d}\Delta[\mathrm{TAl}]/\mathrm{d}t = k_{-2\mathrm{obs}}\Delta[\mathrm{TAl}] - k_{2\mathrm{obs}}([\mathrm{Al}^{3+}]\Delta[\mathrm{T}] + [\mathrm{T}]\Delta[\mathrm{Al}^{3+}]) \quad (36)$$

The conservation of mass can be expressed as

$$\Delta[\mathrm{T}] + \Delta[\mathrm{TAl}] = 0 \quad (37)$$

$$\Delta[\mathrm{AlL}] + \Delta[\mathrm{Al}^{3+}] + \Delta[\mathrm{TAl}] = 0 \quad (38)$$

$$\Delta[\mathrm{AlL}] + \Delta[\mathrm{L}^{3-}] = 0 \quad (39)$$

If eq 6 is assumed rate-limiting, we can write

$$\Delta[\mathrm{TAl}] = [\mathrm{Al}]\Delta[\mathrm{T}]/K_1' + [\mathrm{T}]\Delta[\mathrm{Al}^{3+}]/K_1' \quad (40)$$

If eq 7 is assumed rate-limiting, we can write

$$\Delta A[\mathrm{AlL}] = [\mathrm{L}^{3-}]\Delta[\mathrm{Al}^{3+}]/K_{\mathrm{AlL}} + [\mathrm{Al}^{3+}]\Delta[\mathrm{L}^{3-}]/K_{\mathrm{AlL}} \quad (41)$$

From eq 35 and eqs 37−40, eq 8 is determined, and from eqs 36−39 and eq 41, eqs 8 and 9 are determined.

When TFR and TFe_2 are mixed together, the emission intensity F can be expressed as eq 42.

$$F = f_1[\mathrm{TFR}] + f_2[\mathrm{TFe}_2] + f_3[\mathrm{TFR}-(\mathrm{TFe}_2)_2] \quad (42)$$

From eq 42, the conservation of mass (eqs 43 and 44), and K, eq 23 is determined.

$$c_4 = [\mathrm{TFR}] + [\mathrm{TFR}-(\mathrm{TFe}_2)_2] \quad (43)$$

$$c_1 = 2\,[\mathrm{TFR}-(\mathrm{TFe}_2)_2] + [\mathrm{TFe}_2] \quad (44)$$

f_1 and f_2 were measured for each series of experiments at several TFR and ST concentrations. f_3 was measured at the highest concentrations of c_1 where it was assumed that TFR was saturated with ST. The experiments related to the interaction of TFR with ST were repeated at least five times each, and the uncertainties given ΔK are based on the highest difference detected between the dissociation constants.

ACKNOWLEDGMENT

The authors are grateful to Prof. Philip Aisen for having provided them with his personal protocol for TFR extraction and purification, to Dr. John S. Lomas for constructive discussions, to Dr. Jean-Claude Rouchaud for the CPS experiments, and to Novartis for their gift of desferrioxamine.

REFERENCES

1. Aisen, P., Enns, C., and Wessling-Resnick, M. (2001) Chemistry and biology of eukariotic iron metabolism, *Int. Biochem. Cell Biol. 10*, 940−959.
2. Bruns, C. M., Nowalk, A. J., Arvai, A. S., McTigue, M. A., Vaughan, K. G., Mietzner, T. A., and McRee, D. E. (1997) Structure of Haemophilus influenzae Fe(+3)-binding protein reveals convergent evolution within a superfamily, *Nature Struct. Biol. 4*, 919−924.
3. Zuccola, H. J. The crystal structure of monoferric human serum transferrin, Ph.D. Thesis, Georgia Institute of Technology and University of Michigan, Ann Arbor, 1992.
4. Moore, S. A., Anderson, B. F., Groom, C. R., Haridas, M., and Baker, E. N. (1997) Three-dimensional structure of diferric bovine lactoferrin at 2.8 Å resolution, *J. Mol. Biol. 274*, 222−236.
5. Bou Abdallah, F., and El Hage Chahine, J. M. (1998) Transferrins—hen ovotransferrin, interaction with bicarbonate and iron uptake, *Eur. J. Biochem. 258*, 1022−1031.
6. Dautry-Varsat, A., Ciechanover, A., and Lodish, H. F. (1982) pH and recycling of transferrin during receptor-mediated endocytosis, *Proc. Natl. Acad. Sci. U.S.A. 80*, 2258−2262.
7. Harris, W. R., and Sheldon, J. (1990) Equilibrium constants for binding aluminum to human serum transferrin, *Inorg. Chem. 29*, 119−124.
8. Aramini, J. M., Saponja, J. A., and Vogel, H. J. (1996) Spectroscopic studies of the interaction of aluminum (III) with transferrins, *Coord. Chem. Rev. 149*, 193−229.
9. Martin, R. B., Savory, J., Brown, S., Bertholf, R., and Wills, M. R. (1987) Transferrin binding to Al^{3+} and Fe^{3+}, *Clin. Chem. 33*, 405−407.
10. Cochran, M., Chawtur, V., Jones, M. E., and Marshall, E. A. (1991) Iron uptake by human reticulocytes at physiologic and sub-physiologic concentrations of iron transferrin: the effect of interaction with aluminum transferrin, *Blood 77*, 2347−2353.
11. Cochran, M., Cochran, M., Coates, J. H., and Kurucsev, T. (1987) Direct spectrophotometric determination of the two site binding of aluminum to transferrin, *Life Science 40*, 2337−2341.
12. Ward, R. J., Zhang, Y., and Crichton, R. R. (2001) Aluminum toxicity and iron homeostasis, *J. Inorg. Biochem. 87*, 9−14.
13. Perez, G., Gaarbossa, G., Sassetti, B., Di Risio, C., and Nesse, A. (1999) Interference of aluminum on iron metabolism in erythroleukaemia F562 cells, *J. Inorg. Biochem. 30*, 105−112.
14. Martin, R. B. (1994) Aluminum: a neurotoxic product of acid rain, *Acc. Chem. Res. 27*, 204−210.

15. Abreo, K., Abreo, F., Sella, M. L., and Jain, S. (1999) Aluminum enhances iron uptake and expression of neurofebrility tangle protein in neuroblastoma cells, *J. Neurochem. 75*, 2059−2064.
16. Yokel, R. A., and MacNamara, P. J. (2001) Aluminum toxicokinetics: an updated minireview, *Pharmacol. Toxicol. 88*, 159−167.
17. Yokel, R. A., Allen, D. D., and Ackley, D. C. (1999) The distribution of aluminum in to and out of the brain, *J. Inorg. Biochem. 76*, 127−132.
18. Yokel, R. A. (2000) The toxicology of aluminum in the brain: a review, *Neurotoxicology 21*, 813−828.
19. McGregor, S. J., Naves, M. L., Oria, R., Vass, J. K., and Brock, J. H. (1990) Effect of aluminum on iron uptake and transferrin-receptor expression by human erythroleukaemia K562 cells, *Biochem. J. 272*, 377−382.
20. Clauberg, M., and Joshi, J. G. (1993) Regulation of serine protease activity by aluminum: implication for Alzheimer disease, *Proc. Natl. Acad. Sci. U.S.A. 90*, 1009−1112.
21. Lawrence, C. M., Ray, S., Babyonyshev, M., Galluster, R., Brhani, B. W., and Harrison, S. C. (1999) Crystal structure of the ectodomain of human transferrin receptor, *Science 286*, 779−782.
22. Orberger, G., Fuchs, H., Geyer, R., Gessner, R., Kottgen, E., and Tauber, R. (2001) Structural and functional stability of the mature transferrin receptor from human placenta, *Arch. Biochem. Biophys. 2386*, 79−88.
23. Martell, A. E., Hancock, R. D., Smith, R. M., and Motekaitis, R. J. (1996) Coordination of Al(III) in the environment and in biological systems, *Coord. Chem. Rev. 149*, 311−328.
24. Eigen, M., and DeMaeyer, L. (1963) Relaxation methods. In *Techniques of Organic Chemistry—Investigation of Rates and Mechanism of Reactions, part II* (Friess, S. L., Lewis, E. S., and Weissberger, A., Eds.) Vol 8, pp 895−1029, Wiley-Interscience, New York.
25. Bernasconi, C. F. (1976) *Relaxation Kinetics*, Academic Press, New York.
26. Brouillard, R. (1980) How much may the equilibrium be shifted in a chemical relaxation experiment? *J. Chem. Soc., Faraday Trans. 1 76*, 583−587.
27. Pakdaman, R., Bou Abdallah, F., and El Hage Chahine, J. M. (1999) Transferrin, is a mixed chelate-protein ternary complex involved in the mechanism of iron uptake by serum-transferrin in vitro?, *J. Mol. Biol. 293*, 1273−1284.
28. El Hage Chahine, J. M., and Fain, D. (1993) The mechanism of iron transferrin interactions—Uptake of the iron nitrilotriacetic acid complex, *J. Chem. Soc., Dalton Trans.* 3137−3143.
29. Pakdaman, R., and El Hage Chahine, J. M. (1996) A mechanism for iron uptake by transferrin, *Eur. J. Biochem. 236*, 922−931.
30. Makey, D. G., and Seal, U. S. (1976) The detection of four molecular forms of human transferrin during the iron binding process, *Biochim. Biophys. Acta*, *453*, 250−256.
31. Turkewitz, A. P., Amatruda, J. F., Borhani, D., Harrison, S. C., and Schwartz, A. L. (1988) High yield purification of the human transferrin receptor and properties of its major extracellular fragment, *J. Biol. Chem. 263*, 8318−8325.
32. Bali, P. K., Zak, O., and Aisen, P. (1991) A new role for the transferrin receptor in the release of iron from transferrin, *Biochemistry 30*, 324−328.
33. Tang, S., MacColl, R., and Parsons, P. J. (1995) Spectroscopic study of the interaction of aluminum ions with human transferrin, *J. Inorg. Biochem. 60*, 175−185.
34. Congiu-Castellano, A., Boffi, F., Della Longa, S., Giovannelli, A., Girasole, M., Natali, F., Pompa, M., Soldatov, A., and Bianconi, A. (1997) Aluminum site structure in serum transferrin and lactoferrin revealed by synchrotron radiation X-ray spectroscopy, *Biometals 10*, 363−367.
35. Bellounis, L., Pakdaman, R., and El Hage Chahine, J. M. (1996) Apotransferrin proton dissociation and interactions with bicarbonate in neutral media, *J. Phys. Org. Chem. 9*, 111−118.
36. Schüler, J., Frank, J., Saenger, W., and Georgalis, Y. (1999) Thermally induced aggregation of human transferrin receptor studied by light-scattering techniques, *Biophys. J. 77*, 117−1125.
37. Schüler, J., Frank, J., Trier, U., Schäfer-Korting, M., and Saenger, W. (1999) Interaction kinetics of tetramethylrhodamine transferrin with human transferrin receptor studied by fluorescence correlation spectroscopy, *Biochemistry 38*, 8402−8408.
38. Kubal, G., Mason, A. B., Sadler, P. J., Tucker, A., and Woodworth, R. C. (1992) Uptake of Al^{3+} into the N-lobe of human serum transferrin, *Biochem. J. 285*, 711−714.
39. Sun, H., Cox, M. C., Mason, A. B., Woodworth, A. C., and Sadler, P. J. (1998) [1H, 13C] NMR determination of lobe loading of human serum transferrin: comparison with other metal ions, *FEBS Lett. 422*, 315−320.
40. Bates, G. W., Billups, C., and Saltman, P. (1967) The kinetics and mechanism of iron(III) exchange between chelates and transferrins—the complexes of citrate and nitrilotriacetic acid, *J. Biol. Chem. 242*, 2810−2815.
41. Matzapetakis, M., Kourgiantakis, M., Dakanali, M., Raptopoulou, C. P., Terzis, A., Lakatos, A., Kiss, T., Banyai, I., Iordanidis, L., Mavromoustakos, T., and Salifoglou, A. (2001) Synthesis pH-dependent structural characterization and solution behavior of aqueous aluminum and gallium citrate complexes, *Inorg. Chem. 40*, 1734−1744.
42. Martin, R. B. (1986) Citrate binding to Al^{3+} and Fe^{3+}, *J. Inorg. Biochem. 28*, 181−187.
43. El Hage Chahine, J. M., Bauer, A.-M., Baraldo, K., Lion, C., Ramiandrasoa, F., and Kunesch, G. (2001) Kinetics and thermodynamic of complex formation between Fe^{III} and two synthetic chelators of the dicatecholspermidine family, *Eur. J. Inorg. Chem.* 2287−2296.
44. Roskams, A. J., and Connor, J. R. (1990) Aluminum access to the brain: a role for transferrin and its receptor, *Proc. Natl. Acad. Sci. U.S.A. 87*, 9024−9027.
45. Kawabata, H., Yang, R., Hirama, T., Vuong, P. T., Kawano, S., Gombart, A. F., and Koeffler, H. P. (1999) Molecular cloning of transferrin receptor 2—A new member of the transferrin receptor-like family, *J. Biol. Chem. 274*, 20826−20832.
46. Hirofumi, Y., Tetsuya, S., Kikushi, T., Masahiko, M., and Tadahiro, I. (2000) Molecular modeling of human serum transferrin for rationalizing the changes in its physicochemical properties induced by iron binding—Implication of the mechanism of binding to its receptor, *J. Protein Chem. 19*, 215−223.
47. Kaplan, J., Jordan, I., and Sturrock, A. (1991) Regulation of the transferrin-independent iron transport in cultured cells, *J. Biol. Chem. 266*, 2997−3004
48. Mwanjewe, J., Martinez, R., Agrawal, P., Samson, S. E., Coughlin, M. D., Brassard, P., and Grover, A. K. (2000) On Ca^{2+} dependence of nontransferrin-bound iron uptake in PC12 cells, *J. Biol. Chem. 275*, 33512−33515.
49. Harris, W. R., and Madsen, L. J. (1988) Equilibrium study on the binding of cadmium(II) to human serum transferrin, *Biochemistry 27*, 284−288.
50. Harris, W. R. (1983) Thermodynamic binding constant of the zinc−human transferrin complex, *Biochemistry 22*, 3920−3926.
51. Smith, C. A., Anderson, B. F., Baker, H. M., and Baker, E. N. (1992) Metal substitution in transferrins: the crystal structure of human copper lactoferrin, *Biochemistry 31*, 4527−4533.
52. Gaither, L. A., and Eide, D. J. (2001) Eukaryotic zinc transporters and their regulation, *Biometals 14*, 251−270.
53. Lee, J., Pena, M. M., Nose, Y., and Thiele, D. J. (2002) Biochemical characterization of the human copper transporter Ctrl1, *J. Biol. Chem. 277*, 4380−4387.

BI020627P